

Minimal recipes for global cloudiness

George Datseris¹, Joaquin Blanco², Or Hadas³, Sadrine Bony⁴, Rodrigo Caballero², Yohai Kaspi³, Bjorn Stevens⁴

¹Max Planck Institute for Meteorology, Hamburg, Germany

²Department of Meteorology, Stockholm University, Stockholm, Sweden

³Department of Earth and Planetary Sciences, Weizmann Institute of Science, Rehovot, Israel

⁴Sorbonne University, LMD/IPSL, CNRS, Paris, France

Key Points:

- Model fits are performed to the spatiotemporal observed cloudiness over all oceans, using a minimal set of predictors and parameters
- Models capture global-mean, spatial variability, and mean seasonal cycle of long and shortwave cloud radiative effects
- Cloud albedo and longwave effect are captured by pressure velocity and its variance, surface temperature, and lower tropospheric stability

Corresponding author: George Datseris, george.datseris@mpimet.mpg.de

Abstract

Clouds are primary modulators of Earth’s energy balance. It is thus important to understand the links connecting variabilities in cloudiness to variabilities in other state variables of the climate system, and also describe how these links would change in a changing climate. A conceptual model of global cloudiness can help elucidate these points. In this work we derive simple representations of cloudiness, that can be useful in creating a theory of global cloudiness. These representations illustrate how both spatial and temporal variability of cloudiness can be expressed in terms of basic state variables. Specifically, cloud albedo is captured by a nonlinear combination of pressure velocity and a measure of the low-level stability, and cloud longwave effect is captured by surface temperature, pressure velocity, and standard deviation of pressure velocity. We conclude with a short discussion on the usefulness of this work in the context of global warming response studies.

Plain Language Summary

Clouds are important for Earth’s climate, because they affect a large portion of the planet’s energy balance, and hence its mean temperature. To better understand how the interplay between cloudiness and energy balance would change in a changing climate, we need a better theoretical understanding of how many clouds are distributed over the planet, and how this connects with the state variables of the climate system such as temperature and wind speed. As our theoretical understanding is currently limited, in this work we illustrate the simplest way one could represent the spatiotemporal distribution of clouds over the whole planet. We believe that these simple representations will pave the way for a conceptual theory of global cloudiness and its impact on the energy balance. We show that the impact of cloudiness on both solar and terrestrial radiation balance can be captured well with only a few predictive fields, like surface temperature or vertical wind speed, combined simply and using only three tunable parameters.

1 Introduction

Clouds are one of the most fascinating, important, and complex components of Earth’s climate system (Siebesma et al., 2020). Despite their importance, we lack theoretical understanding of what controls planetary-wide cloudiness. For example, while we have a good understanding of the microphysics of cloud generation and radiative transfer through clouds (Houze, 2014; Cotton et al., 2014; Siebesma et al., 2020), it is difficult to use these theories to make claims about global cloudiness. Earth System Models (ESMs) and other bottom-up approaches do couple cloud formation to the global circulation. However, so far they have not been proven effective in constraining global cloudiness variability (Sherwood et al., 2020; Zelinka et al., 2020). This makes it difficult to transparently establish links between variability in global cloudiness and Earth’s energy balance, or how this link would change in a changing climate.

Conceptual models could be useful in elucidating how the main features of cloudiness connect to the energy balance, and how these connections may respond to large scale climatic changes. However, existing conceptual work on large-scale cloudiness is sparse. The majority of theory relevant to cloudiness is about the general circulation. Existing work has focused on specific regions or regimes, such as the tropics (Pierrehumbert, 1995; Miller, 1997), the Walker circulation (Peters & Bretherton, 2005), or the formation of midlatitude storms (Charney, 1947; Eady, 1949; Pierrehumbert & Swanson, 1995), among others, and further research may link circulation with cloud formation at large, but still local, scales (Carlson, 1980). What is missing is a conceptual framework that both closes the top-of-atmosphere energy budget (and hence by necessity considers the planet as a whole), but also includes clouds. A suitable candidate for such a framework would be

64 a an energy balance model (Budyko, 1969; Sellers, 1969; Ghil, 1981; North & Kim, 2017)
65 that explicitly represents dynamic cloudiness.

66 In this work we derive simple representations, or “recipes”, for global cloudiness,
67 which can be potentially included in energy balance models, helping link variations in
68 the energy budget and state variables of such models to variations in cloudiness and vice-
69 versa. These representations therefore need to capture all main features of cloudiness,
70 which are the global mean value, mean seasonal cycle, coarse spatial variability, and the
71 difference between the shortwave and longwave impact of cloudiness. To derive them,
72 we will use a quantitative top-down approach, where global cloudiness is directly decom-
73 posed into contributions from several simpler spatiotemporal fields. These fields are the
74 “ingredients” of the recipe, which we refer to simply as predictors (in the sense of sta-
75 tistical predictors). A model useful in theoretical work is one that can explain the most
76 with the least amount of information, and therefore in this work the main objective is
77 to derive minimal representations that use a few predictors.

78 Similar top-down approaches have been used frequently in the literature in the con-
79 text of the empirical cloud controlling factors framework (Stevens & Brenguier, 2009).
80 For tropical low clouds there are several studies summarized in the review by Klein et
81 al. (2017), and see also Myers et al. (2021) for ESMs vs. observations. Attention has also
82 been given to the midlatitude cloudiness (a summary of existing work on extratropical
83 cloud controlling factors can be found in Kelleher and Grise (2019) and see also Grise
84 and Kelleher (2021) for ESMs vs. observations). Our approach differs from past empir-
85 ical approaches in that we fit absolute cloudiness, not anomalies, and we fit cloudiness
86 fields over all available space and time.

87 Section 2 describes how we define cloudiness, which predictors to consider, how to
88 fit predictor models on observed cloudiness, and how to judge the quality of the fits. Then,
89 Sect. 3 presents the main analysis and results on how well the models capture cloud albedo
90 and cloud longwave radiative effect. A summary and discussion of potential impact for
91 sensitivity studies concludes the paper in Sect. 4.

92 **2 Fitting global cloudiness**

93 **2.1 Quantifying cloudiness**

94 To fit any model, a definition of cloudiness that is both quantitatively precise but
95 also energetically meaningful is required. For the shortwave part, we use the energeti-
96 cally consistent effective cloud albedo (in the following, just “cloud albedo”), C , estimated
97 using the approach of Datsersis and Stevens (2021). C is a better way to quantify short-
98 wave impact of cloudiness than the shortwave cloud radiative effect (CRE), because a
99 large amount of variability of the latter actually comes from the variability of insolation
100 (Datsersis & Stevens, 2021). For the longwave part the CRE, L , is a good representation
101 of the radiative impact of clouds. From it, a cloud effective emissivity can be constructed
102 which can be added to an energy balance model directly similarly to the albedo. Both
103 C, L are derived from monthly-mean CERES EBAF data (Loeb et al., 2018) using 19
104 years of measurements (2001-2020).

105 **2.2 Predictors considered**

106 The predictors considered in this study, listed below, are obtained from ERA5 data
107 (Hersbach et al., 2020) using 19 years of data (2001-2020). Pressure velocity ω_{500} , es-
108 timated inversion strength EIS, surface wind speed V_{sf} , sea surface temperature SST,
109 and stratospheric specific humidity q_{700} , have been used numerous times in the litera-
110 ture. ω_{500} is known to be important for both shortwave and longwave cloud radiative
111 effects (Bony et al., 1997; Norris & Weaver, 2001; Bony et al., 2004; Norris & Iacobel-

lis, 2005), and EIS, V_{sfc} , SST, q_{700} have been used to fit cloud cover anomalies in a variety of regimes, see e.g., Klein et al. (2017); Kelleher and Grise (2019) and references therein for a more detailed discussion. Do note that the connections between predictors and cloudiness in the literature are analyzed for specific regimes (such as tropical subsidence regions, or North midlatitudes, etc.), while here we depart from past work by testing their potential in fitting cloudiness globally.

We included CTE, the estimated cloud top entrainment index, because Kawai et al. (2017) present it as an improvement over EIS. Both q_{700} , q_{tot} (with q_{tot} the total column water vapor) are a proxy for the moisture of an atmospheric column, and expected to be relevant when fitting L . In our analysis however, q_{700} gives consistently better fits when used in place of q_{tot} , keeping all other aspects fixed (not shown). Thus, we will not discuss q_{tot} more in this study. Using specific humidity at 700hPa instead of at surface results in only minor improvement of fit quality throughout the analysis (also not shown).

The fraction of updrafts ω_{up} is useful because it is bounded in $[0\%, 100\%]$, like C , and given that we fit absolute values instead of anomalies, it does not penalize the fits with negative values (that exist in ω_{500}). It can also be used as a statistical weight to distinguish between regions of large scale subsidence, see e.g., Bony et al. (1997). The standard deviation of ω_{500} , ω_{std} , which can be thought of as a simple quantifier of storminess, has been shown to be a useful predictor of cloudiness by Norris and Iacobellis (2005) due to the nonlinear connection between vertical motion and cloud generation. Another argument favoring ω_{std} is that it relates cloudiness with the moisture of the air column better than ω_{500} , see Sect. 3.3.

2.3 Fitting process

Let Y be a measure of cloudiness (C or L from Sect. 2.1) and X_i be some predictor fields, for $i = 1, \dots, n$. Y, X_i are global spatiotemporal fields. We assume that with sufficient accuracy we can write

$$Y \approx M = f(X_1, \dots, X_n; p_1, \dots, p_m) \stackrel{\text{e.g.}}{=} p_1 X_1 + p_2 X_2 + p_3 X_1 X_2 \quad (1)$$

with p_j , for $j = 1, \dots, m$ some parameters to be estimated (all $p_j \in \mathbb{R}$). In the following we call f the “cloud fitting function”. Naturally, different forms for f and/or sets of predictors will yield a better fit for C or L respectively, as each captures different aspects of cloudiness. Given a specific form for f , and a set of predictors X_i , the parameters p_j of the model are estimated via a standardized nonlinear least square optimization (Levenberg, 1944; Marquardt, 1963). The minimization objective is the squared distance between Y derived from CERES observations, and M produced by Eq. 1. Details on the data pre-processing before doing the fits are provided in the Supplementary Information.

This approach of fitting models with free parameters to observed data is similar to the cloud controlling factors framework (CCFF), but there are some key differences with typical CCFF studies. First, we fit absolute cloudiness, not anomalies, and hence the mean value of Y , and its seasonal cycle, must be captured by the fit. The importance of capturing the mean value and mean seasonal cycle is further enforced by the fact that the inter-annual variability of cloudiness is small in decadal timescales (Stevens & Schwartz, 2012; Stephens et al., 2015), and hence the mean seasonal cycle captures the majority of the signal. Because we want to capture the mean, f is generally allowed to be nonlinear. Second, we fit across all available space and time without any restrictions to special regions of space or specific cloud types. We discuss in more detail the differences with typical CCFF studies in the Supplementary Information.

158

2.4 Quantitatively measuring fit quality

159

160

To quantify fit quality with an objective measure that is independent of what predictors are used, we chose the normalized root mean square error (NRMSE), defined as

$$\epsilon(Y, M) = \sqrt{\frac{\sum_n (Y_n - M_n)^2}{\sum_n (Y_n - \bar{Y})^2}} \quad (2)$$

161

162

163

164

165

166

167

168

169

with Y, M as in Eq. 1, \bar{Y} the mean of Y and n enumerates the data points. This error measure is used routinely in e.g., spatiotemporal timeseries prediction (Isensee et al., 2019), and is a statistic agnostic of the values of Y, M that can compare fit quality across different ways of fitting. If $\epsilon > 1$ the mean value of Y is a better model than M (equivalently, the variance of the observations is smaller than the mean square error between fit and observations). There are several ways to compute ϵ : on full spatiotemporal data, on zonally and temporally averaged data, or on the seasonal cycles of tropics (0° - 30°) and midlatitudes (30° - 70°). Each measure highlights a different aspect of fit quality and all measures were taken into account when deciding the best fits.

170

3 Results & Discussion

171

172

173

174

175

176

177

178

In this section we present the “best” fits for cloud albedo C and longwave cloud radiative effect L . The “best” fits are the most minimal fits, that accommodate intuitive physical justification, but also provide good fit quality (i.e., low values for ϵ). Only the requirement is small error ϵ is objective, while the rest have at least partly a subjective nature. Additionally, fits that use simpler predictors, that can be more straightforwardly represented in a conceptual framework, are preferred. If two fits have approximately equal error ϵ , but one uses a simpler predictor (e.g., surface temperature SST versus atmospheric specific humidity q_{700}), the first fit is “better”.

179

3.1 Two predictor linear model

180

181

182

183

184

185

186

187

188

The simplest model one can use for the cloud fitting function f is one that combines two predictors and two free parameters in a linear manner: $f = p_1 X_1 + p_2 X_2$. Even if this model does not yield a good fit for cloudiness, it is advantageous to start with it nevertheless. All possible linear combinations given all possible predictors of Sect. 2.2 are only 36, and they can already highlight which predictors are worth a closer look for which measure of cloudiness. The results are in Fig. 1, which showcases two different error measures (error in temporally and zonally mean cloudiness, and median of errors in seasonal cycle of cloudiness), and how these errors depend on which predictors are used for the linear fit.

189

190

191

192

193

194

The majority of combinations result in low fit quality ($\epsilon \geq 0.9$). Nevertheless, Fig. 1 reveals some useful information. For C , a measure of the inversion strength is necessary for a decent fit and the combination of ω_{up} and CTE result in the best case scenario. For L , the most important predictor seems to be ω_{std} , which gives decent fits in both space and time for a wide selection of second predictors (while ω_{500} gives decent fits only in time). A second important predictor for L seems to be q_{700} or SST.

195

3.2 Best fit for cloud albedo C

196

197

198

199

200

201

While it is already clear in the literature that ω_{500} is an important predictor for shortwave impact of clouds (Sect. 2.2), the fact that ω_{up} performs so much better in a linear model hints that the bounded nature of albedo, $C \in [0\%, 100\%]$, is important. Negative predictor values yield low fit quality and also penalize fitting well positive values. One way to counter this would be to use ω_{up} as probability weight multiplying other predictors. An alternative would be to use appropriate nonlinear functions of the more

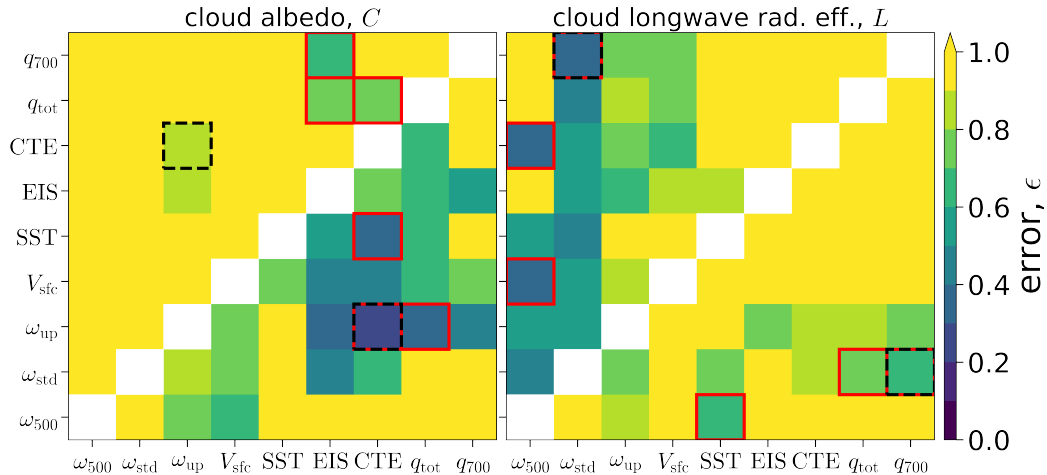


Figure 1. Error in temporally and zonally mean cloudiness (lower-right triangle of heatmap), and error in mean seasonal cycle (upper-left triangle of heatmap), as a function of which predictors of the x and y axis combine into a linear model $f = p_1 X_1 + p_2 X_2$ for fitting cloud albedo (left plot) or longwave cloud radiative effect (right plot). Red outline highlights the three combinations with the lowest error in each category, while black dashed outline highlights the combination with lowest error overall (by multiplying the two errors). It is possible that $e > 1$ because we are fitting without intercept.

202 basic ω_{500} . Regardless the choice, CTE must also be included in the model, as it is nec-
 203 cessary to capture the important contribution of low clouds.

204 A model that satisfies all these requirements, and achieves the best fit, is

$$C = 50p_1 (\tanh(p_2\omega_{500} + p_3\text{CTE}) + 1) \quad (3)$$

205 where we used the nonlinear function $x \rightarrow 50(\tanh(x)+1)$ to map predictors to [0%, 100%].
 206 The results of the fit (i.e., estimating the parameters p_1, p_2, p_3 that give least square er-
 207 ror between Eq. 3 and the observed CERES C) are in Fig. 2. The model fit captures all
 208 main features of cloud albedo, and achieves $\epsilon = 0.54$ over the full space and time, $\epsilon =$
 209 0.19 in the zonal and temporal average, and $\epsilon = 0.65$ in seasonal cycle. The shortwave
 210 cloud radiative effect (which in our study is simply the multiplication of C with the in-
 211 solation I , and then averaging), is 57.1 W/m^2 in CERES and 57.45 W/m^2 when using
 212 the model fit. The inclusion of the parameter p_1 is necessary, because in observations
 213 cloud albedo does not saturate to 100%, but to much lower values (see Fig. 2). We also
 214 note that using EIS instead of CTE in the model decreases fit quality significantly, be-
 215 cause, while EIS and CTE both capture subtropical low cloud albedo well, only CTE also
 216 captures midlatitude low cloud albedo well, while EIS does not. Thus, as suggested by
 217 Kawai et al. (2017), CTE is indeed an improvement over EIS.

218 Adding more predictors increases fit quality only slightly. E.g., adding a factor $p_4 V_{\text{sfc}}$
 219 inside the tanh function decreases time and zonal mean error to $\epsilon = 0.18$ from $\epsilon = 0.19$
 220 and seasonal cycle error to $e = 0.6$ from $e = 0.65$, as well as captures hemispheric asym-
 221 metries in C slightly better. That the decrease in error is so small gives confidence that
 222 that the basic physics governing cloud albedo are already captured by Eq. 3. Further fine-
 223 tuning of the model only captures higher order details that will likely not be included
 224 in a conceptual theory anyway.

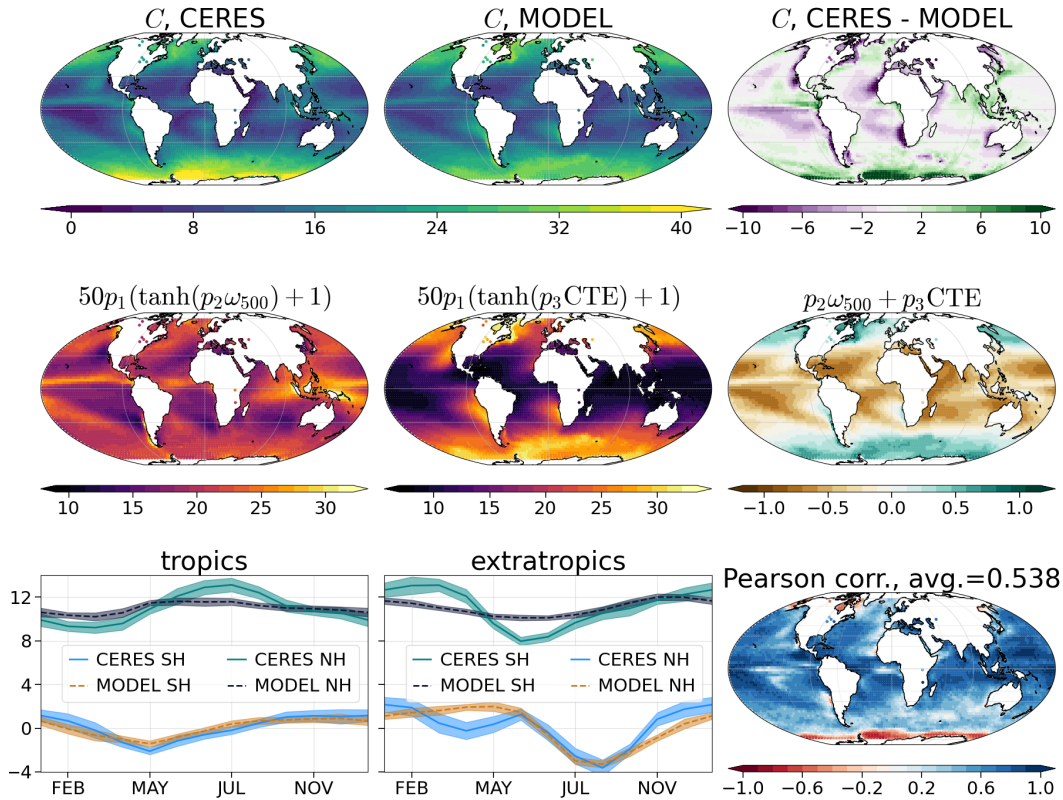


Figure 2. Results of fitting cloud albedo C (units of %) with the simple model of Eq. 3. First row are time-averaged maps. See also Fig. 4 for a zonally averaged version. Second row are the contributions of different terms in the model. Third row shows how well the model captures temporal variability. First two panels are the mean seasonal cycles (with semi-transparent bands noting the standard deviation around each month) in the tropics ($0-30^\circ$) and extratropics ($30-70^\circ$). The mean value of all cycles has been subtracted, and SH cycles are offset for visual clarity. The third panel is a map of the Pearson linear correlation coefficient between the time-series of the model and CERES data at each grid point. Units of ω_{500} in Pa/s and CTE in K, and $p_1 = 0.4, p_2 = 6.87, p_3 = 0.08$. We multiply ω_{500} with -1 before any analysis so that $\omega_{500} > 0$ means updrafts.

225 The middle row of Fig. 2 provides some insights on the contribution of each predictor.
 226 Both CTE and ω_{500} contribute to midlatitude cloud albedo, but CTE slightly
 227 more so. In the tropics ω_{500} contributes the albedo of the convective regimes (ITCZ, Mar-
 228 itime Continent), and CTE the albedo of the low stratocumulus decks (subsidence re-
 229 gions). CTE is in some sense a more important predictor than ω_{500} , because if we set
 230 explicitly $p_2 = 0$ in Eq. 3, we get lower error of $\epsilon = 0.7$ in full space and time, ver-
 231 sus the error of $\epsilon = 0.9$ we would get if we set explicitly $p_3 = 0$ instead. Alternative
 232 models to Eq. 3 can give similar results using ω_{up} instead of ω_{500} . For example, using
 233 $f = p_1\omega_{up} + p_2CTE(1 - \omega_{up})$ provides similar, but slightly worse, fit quality with $\epsilon =$
 234 0.57 over full space and time and $\epsilon = 0.23$ over time and zonal mean. However, ω_{500}
 235 is a simpler predictor than ω_{up} , and hence a model with ω_{500} is more minimal (and thus,
 236 “better”).

3.3 Best fit for longwave cloud radiative effect L

Fitting L is more complex for mainly two reasons. First, the longwave effect of a cloud depends strongly on the infrared opacity, and hence moisture content, of the atmospheric column overshadowed by the cloud. Moisture content though is, at least partly, controlled by temperature. Warm and humid atmospheres are already almost opaque to longwave radiation, and hence the presence of a cloud would make little difference. In contrast, in a cold and dry atmosphere a cloud would bring a lot of extra absorption of outgoing longwave radiation and hence large L . Second, cloud height matters a lot for its effective emissivity (as cloud height sets its temperature), while cloud height does not have a significant effect on cloud albedo (keeping all other factors fixed).

These considerations likely explain why we were not able to find a model that had as good of a fit for L as it had for C when restricting the model to using at most two predictors. After an analysis of several different linear and nonlinear combinations, the “best” model we could construct was of the form

$$L = p_1\omega_{\text{std}} + p_2\omega_{500} + p_3\text{SST} \quad (4)$$

(notice how Eq. 4 has 0 intercept by force, so that it must capture the mean from the predictors, and not from a tunable parameter). The results of the fit are in Fig. 3. Similarly with C , the fit captures all main features of L . The fit errors are $e = 0.63$ over full space and time, $e = 0.46$ in time and zonal mean and $e = 0.41$ in mean seasonal cycle. The mean LCRE is 27.27 W/m^2 in CERES and 27.30 in our model fit W/m^2 . Spatial variability is captured worse for L versus C , but temporal variability is captured better. A factor that contributes to this is that the temporal variability of L is much simpler than it is for C (e.g., relative power of 12-month periodic component is much larger in L timeseries, leading to simpler seasonal cycle temporal structure).

We now give some physical intuition on the choice of predictors. Monthly-mean ω_{500} is a proxy to cloud height (persistent updrafts and with larger magnitude should result in higher clouds). The surface temperature SST is a proxy for the emissivity of the air column without a cloud, because the potential total moisture content of atmospheric columns is a monotonically increasing function of temperature under first approximation. Using q_{700} instead of SST captures spatial variability worse but improves the capturing of temporal variability. Given that SST is a more basic predictor than q_{700} , and is directly represented in conceptual energy balance models, SST is preferred. Furthermore, and as was the case with C , adding more predictors, or additional nonlinear terms of existing predictors such as a factor $p_4\omega_{\text{std}}\text{SST}$, increases fit quality but only slightly.

Interestingly, ω_{std} is the most important predictor for L . Even though ω_{500} captures a broader range of values (~ 40 versus the ~ 30 of ω_{std}), absence of ω_{std} significantly lowers fit quality in all combinations of cloud fitting functions f and predictors we tested, even when including ω_{500} in all of them. The spatial structure of ω_{std} is the most similar to the spatial structure of L , with the main difference being that for ω_{std} the peak values in tropics and extratropics have equal magnitude, while for L the tropics peak values have 33% more magnitude. Hence, some other predictor must lower the extratropical magnitude of ω_{std} , and here this role is fulfilled by SST in Eq. 4 (or q_{700} , if one uses it instead of SST).

A physical connection between ω_{std} and L can be thought of as follows: persistent updrafts, that are captured by ω_{500} , lead to a moist atmosphere and hence weak L , mostly irrespectively of cloud height. On the other hand, consistent pumping of air up and down (high ω_{std} , but almost zero ω_{500}) would leave the atmosphere dry (for at least half the time), but the formed clouds would linger longer above the dry atmosphere and have a disproportionately strong effect, yielding high L . In the midlatitudes both L and ω_{std} have their latitudinal maximum in the middle of the Ferrel cell ($40\text{-}45^\circ$), where $\omega_{500} \approx 0$. Of course, monthly-mean $\omega_{500} \approx 0$, but in the hourly timescale there is a lot of ver-

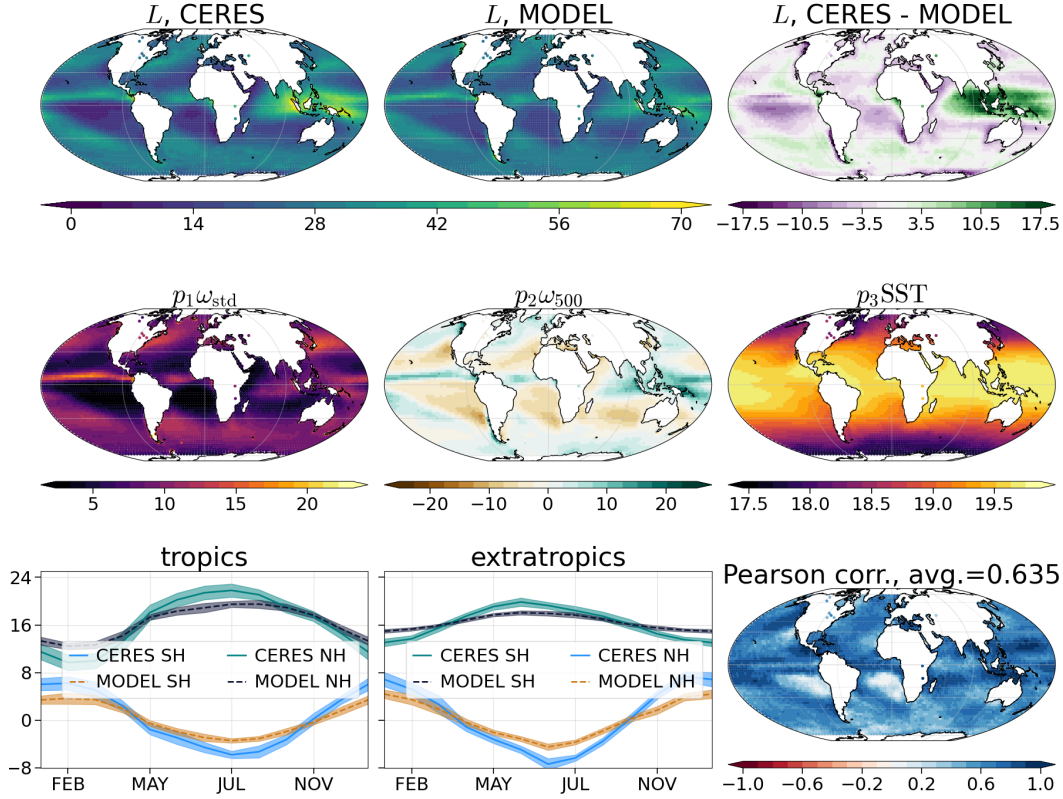


Figure 3. As in Figure 2 but now for longwave cloud radiative effect L . Units of L in W/m^2 , $\omega_{500}, \omega_{\text{std}}$ in Pa/s , SST in K, and $p_1 = 42.68, p_2 = 208.9, p_3 = 0.06558$.

287 tical motion, as captured by the high values of ω_{std} . This reflects the fact that the center
 288 of the Ferrell cell coincides with the centre of the midlatitude storm tracks. In the
 289 tropics, ω_{500} and ω_{std} have little differences in their latitudinal structure.

290 3.4 Comparison with ERA5 and reduced data

291 For obtaining reference values of the errors we report here, we also compare the out-
 292 come of our analysis with using direct ERA5 radiation output to measure C or L . Cal-
 293 culating L is straightforward, however, we cannot compute the energetically consistent
 294 effective cloud albedo from ERA5, because it requires cloud optical depth, a field not ex-
 295 ported by ERA5. Instead, we can compute the cloud contribution to atmospheric albedo
 296 α^{CLD} (specifically, Eq. 3 from Datsersis and Stevens (2021)), which has only small dif-
 297 ferences with C . α^{CLD} also has the downside of not having a time dimension due to ab-
 298 sence of sunlight for large portions of the data (Datsersis & Stevens, 2021).

299 We also present fits and their errors for fitting reduced data directly, specifically
 300 temporally and zonally averaged data. Fitting reduced data increases fit quality, because
 301 this case neglects higher-order effects that contribute to e.g. zonal or temporal structure.
 302 If, however, the fit quality increases only slightly, that gives confidence that the basic con-
 303 nections captured by our models are indeed the most important ones and hence also domi-
 304 nate full spatiotemporal variability. The results are in Fig. 4.

305 Two conclusions can be readily drawn: (1) our fits have smaller error ϵ than does
 306 the cloudiness inferred from ERA5 radiation output, (2) fitting the simplified version of

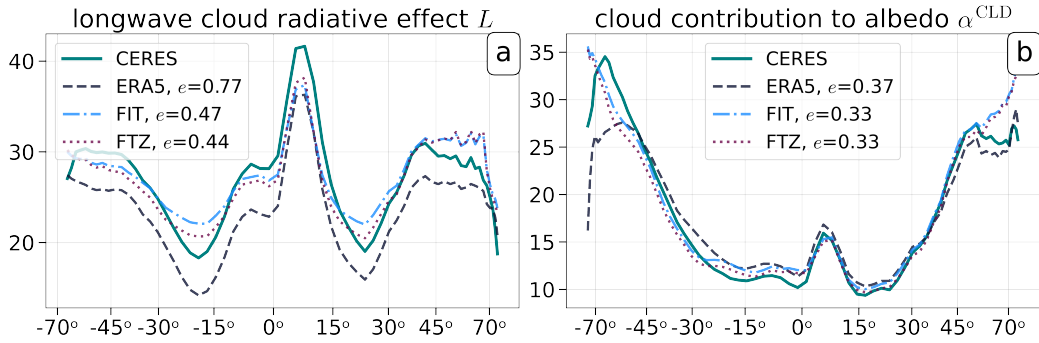


Figure 4. Temporally and zonally averaged data (and their errors e , Eq. 2, versus the CERES curve) of CERES, our model fits, and direct ERA5 output for (a) the longwave cloud radiative effect L and (b) the cloud contribution to atmospheric albedo α^{CLD} . In (a), “FIT” is over all space and time, and “FTZ” is a fit over temporally and zonally averaged data. In (b), “FIT” is a fit over temporally averaged data (no time information can be used), and “FTZ” is as before.

temporally and zonally averaged data increases fit quality only slightly, further validating the fit quality. Additionally, the best parameters of the fits change little when doing the zonal-only fit (e.g., for C , parameters become $p_1 = 0.4, p_2 = 8.25, p_3 = 0.077$ versus those reported in Fig. 2). This means that the contribution of each predictor does not change fundamentally in the reduced version, giving us even more confidence that the simple models of Eqs. 3, 4 capture the basic physics well.

4 Conclusions

The goal of this work was to identify ways one can accurately represent observed global cloudiness using as few and as simple components as possible. We have shown that the combination of pressure velocity ω_{500} and a measure of temperature inversion CTE are enough to capture all main features of cloud albedo, while surface temperature SST, standard deviation of hourly pressure velocity ω_{std} , and ω_{500} , capture all main features of longwave cloud radiative effect. Our model fits naturally have some discrepancies with observations, but none are major. E.g., southern ocean C is underestimated, temporal variability of C is not captured well, especially in southern ocean, L of Maritime Continent is underestimated, among others. Even though we only fitted over ocean here, in fact the fits do not perform much worse when considering the whole planet without adding more information to the cloud fitting functions f (not shown). We also note that the predictors used in the presented models were favored because of their simplicity, but also because they can be potentially connected with equator-to-pole temperature gradients. This may allow incorporating cloudiness in energy balance models, a possibility which we outline in the Supplementary Information.

Equations 3 and 4, and the analysis of Sect. 3, can also be used to quantify the response of cloudiness to a change in the climate system. For example, quantify how a change in the variability of the circulation or inversion strength would impact global cloudiness and hence the energy balance. But also, the equations can provide spatially localized information on such changes, such as in which areas of the globe would circulation changes impact global cloudiness the most. These applications seem useful for e.g., better quantifying cloud sensitivities in the context of global warming.

336 The exact parameter values p_j in Eqs. 3 and 4 have been derived from fitting on
337 current climate and their values may change for different climates. Thankfully, this change
338 is not very large. We confirmed that by doing the fit of Sect. 3.2, but for each hemisphere
339 individually. As far as circulation patterns and cloudiness distributions are concerned,
340 the two hemispheres have significant differences. Recall that the parameters of the fit
341 for the whole globe were $p = \{0.4, 6.87, 0.08\}$. For only north hemisphere, we obtained
342 $\{0.38, 7, 0.07\}$ and for only south $\{0.41, 6.89, 0.086\}$. Because the parameter sets have
343 little differences in each case, this gives more confidence that the equations capture the
344 basic physical connections instead of being a case of overfitting.

345 Acknowledgments

346 We thank Hauke Schmidt for helpful discussions. The datasets used were monthly mean
347 CERES EBAF (Loeb et al., 2018; Kato et al., 2018; Doelling et al., 2013; Rutan et al.,
348 2015) for surface & top of the atmosphere radiation fields, and cloud properties, monthly
349 mean ERA5 (Hersbach et al., 2020) for temperature, pressure, humidity, and hourly mean
350 ERA5 for pressure velocity. The code we used is available online (Datseris, 2022). It uses
351 the Julia language (Bezanson et al., 2017), and the packages: GLM.jl, LsqFit.jl, Climate-
352 Base.jl, and DrWatson (Datseris et al., 2020). Figures were produced with the matplotlib
353 library (Hunter, 2007). The code can also be used to fit any arbitrary spatiotemporal
354 field with any combination of functional forms and predictor fields.

355 **Author contributions.** G.D. performed the primary analysis and wrote the first draft.
356 All authors contributed key ideas that shaped the study, and helped revise the draft.

357 References

- 358 Bezanson, J., Edelman, A., Karpinski, S., & Shah, V. B. (2017). Julia: A fresh ap-
359 proach to numerical computing. *SIAM Review*, 59(1), 65–98. Retrieved from
360 <https://epubs.siam.org/doi/10.1137/141000671> doi: 10.1137/141000671
- 361 Bony, S., Dufresne, J.-L., Treut, H. L., Morcrette, J.-J., & Senior, C. (2004, March).
362 On dynamic and thermodynamic components of cloud changes. *Climate Dy-*
363 *namics*, 22(2-3), 71–86. Retrieved from <https://doi.org/10.1007/s00382>
364 [-003-0369-6](https://doi.org/10.1007/s00382-003-0369-6) doi: 10.1007/s00382-003-0369-6
- 365 Bony, S., Lau, K.-M., & Sud, Y. C. (1997). Sea surface temperature and large-
366 scale circulation influences on tropical greenhouse effect and cloud radia-
367 tive forcing. *Journal of Climate*, 10(8), 2055 - 2077. Retrieved from
368 <https://journals.ametsoc.org/view/journals/clim/10/8/1520-0442>
369 [_1997_010_2055_sstals.2.0.co.2.xml](https://journals.ametsoc.org/view/journals/clim/10/8/1520-0442_1997_010_2055_sstals.2.0.co.2.xml) doi: 10.1175/1520-0442(1997)010<2055:
370 SSTALS>2.0.CO;2
- 371 Budyko, M. I. (1969). The effect of solar radiation variations on the climate of the
372 Earth. *Tellus*, 21(5), 611–619. doi: 10.3402/tellusa.v21i5.10109
- 373 Carlson, T. N. (1980). Airflow through midlatitude cyclones and the comma
374 cloud pattern. *Monthly Weather Review*, 108(10), 1498 - 1509. Re-
375 trieved from <https://journals.ametsoc.org/view/journals/mwre/>
376 [108/10/1520-0493_1980_108_1498_atmcat_2_0_co_2.xml](https://journals.ametsoc.org/view/journals/mwre/108/10/1520-0493_1980_108_1498_atmcat_2_0_co_2.xml) doi: 10.1175/
377 1520-0493(1980)108(1498:ATMCAT)2.0.CO;2
- 378 Charney, J. G. (1947, oct). The dynamics of long waves in a baroclinic westerly
379 current. *Journal of the Atmospheric Sciences*, 4(5), 136–162. Retrieved from
380 [http://journals.ametsoc.org/doi/10.1175/1520-0469\(1947\)004%3C0136:
381 TDOLWI%3E2.0.CO;2](http://journals.ametsoc.org/doi/10.1175/1520-0469(1947)004%3C0136:TDOLWI%3E2.0.CO;2) doi: 10.1175/1520-0469(1947)004<0136:TDOLWI>2.0.CO;
382 2
- 383 Cotton, W. R., Bryan, G., & Van Den Heever, S. C. (2014). *Storm and cloud dy-*
384 *namics* (2nd ed.). Academic Press.
- 385 Datseris, G. (2022). *Code for our paper “minimal recipes for global cloudiness”*. Zen-
386 odo. doi: 10.5281/zenodo.6565962

- 387 Datseris, G., Isensee, J., Pech, S., & Gál, T. (2020). Drwatson: the perfect side-
388 kick for your scientific inquiries. *Journal of Open Source Software*, 5(54), 2673.
389 Retrieved from <https://doi.org/10.21105/joss.02673> doi: 10.21105/joss
390 .02673
- 391 Datseris, G., & Stevens, B. (2021, August). Earth’s albedo and its symmetry. *AGU*
392 *Advances*, 2(3). Retrieved from <https://doi.org/10.1029/2021av000440>
393 doi: 10.1029/2021av000440
- 394 Doelling, D. R., Loeb, N. G., Keyes, D. F., Nordeen, M. L., Morstad, D., Nguyen,
395 C., ... Sun, M. (2013, June). Geostationary enhanced temporal inter-
396 polation for CERES flux products. *Journal of Atmospheric and Oceanic*
397 *Technology*, 30(6), 1072–1090. Retrieved from [https://doi.org/10.1175/](https://doi.org/10.1175/jtech-d-12-00136.1)
398 [jtech-d-12-00136.1](https://doi.org/10.1175/jtech-d-12-00136.1) doi: 10.1175/jtech-d-12-00136.1
- 399 Eady, E. T. (1949). Long waves and cyclone waves. *Tellus*, 1(3), 33–52.
- 400 Ghil, M. (1981). Energy-Balance Models: An Introduction. In *Climatic varia-*
401 *tions and variability: Facts and theories* (pp. 461–480). Dordrecht: Springer
402 Netherlands. Retrieved from [http://link.springer.com/10.1007/](http://link.springer.com/10.1007/978-94-009-8514-8_27)
403 [978-94-009-8514-8_27](http://link.springer.com/10.1007/978-94-009-8514-8_27) doi: 10.1007/978-94-009-8514-8_27
- 404 Grise, K. M., & Kelleher, M. K. (2021). Midlatitude cloud radiative effect sensitiv-
405 ity to cloud controlling factors in observations and models: Relationship with
406 southern hemisphere jet shifts and climate sensitivity. *Journal of Climate*,
407 34(14), 5869–5886. doi: 10.1175/JCLI-D-20-0986.1
- 408 Hersbach, H., Bell, B., Berrisford, P., Hirahara, S., Horányi, A., Muñoz-Sabater,
409 J., ... Thépaut, J.-N. (2020, June). The ERA5 global reanalysis. *Quarterly*
410 *Journal of the Royal Meteorological Society*, 146(730), 1999–2049. Retrieved
411 from <https://doi.org/10.1002/qj.3803> doi: 10.1002/qj.3803
- 412 Houze, R. A., Jr. (2014). *Cloud dynamics* (2nd ed.). Academic Press.
- 413 Hunter, J. D. (2007). Matplotlib: A 2d graphics environment. *Computing in Science*
414 *& Engineering*, 9(3), 90–95. doi: 10.1109/MCSE.2007.55
- 415 Isensee, J., Datseris, G., & Parlitz, U. (2019, October). Predicting spatio-
416 temporal time series using dimension reduced local states. *Journal of Non-*
417 *linear Science*, 30(3), 713–735. Retrieved from [https://doi.org/10.1007/](https://doi.org/10.1007/s00332-019-09588-7)
418 [s00332-019-09588-7](https://doi.org/10.1007/s00332-019-09588-7) doi: 10.1007/s00332-019-09588-7
- 419 Kato, S., Rose, F. G., Rutan, D. A., Thorsen, T. J., Loeb, N. G., Doelling, D. R.,
420 ... Ham, S.-H. (2018, May). Surface irradiances of edition 4.0 clouds and the
421 earth’s radiant energy system (CERES) energy balanced and filled (EBAF)
422 data product. *Journal of Climate*, 31(11), 4501–4527. Retrieved from
423 <https://doi.org/10.1175/jcli-d-17-0523.1> doi: 10.1175/jcli-d-17-0523.1
- 424 Kawai, H., Koshiro, T., & Webb, M. J. (2017, November). Interpretation of
425 factors controlling low cloud cover and low cloud feedback using a unified
426 predictive index. *Journal of Climate*, 30(22), 9119–9131. Retrieved from
427 <https://doi.org/10.1175/jcli-d-16-0825.1> doi: 10.1175/jcli-d-16-0825.1
- 428 Kelleher, M. K., & Grise, K. M. (2019). Examining Southern Ocean cloud
429 controlling factors on daily time scales and their connections to midlat-
430 itude weather systems. *Journal of Climate*, 32(16), 5145–5160. doi:
431 10.1175/JCLI-D-18-0840.1
- 432 Klein, S. A., Hall, A., Norris, J. R., & Pincus, R. (2017). Low-Cloud Feedbacks
433 from Cloud-Controlling Factors: A Review. *Surveys in Geophysics*, 38(6),
434 1307–1329. doi: 10.1007/s10712-017-9433-3
- 435 Levenberg, K. (1944). A method for the solution of certain non-linear problems in
436 least squares. *Quarterly of Applied Mathematics*, 2(2), 164–168. Retrieved
437 from <https://doi.org/10.1090/qam/10666> doi: 10.1090/qam/10666
- 438 Loeb, N. G., Doelling, D. R., Wang, H., Su, W., Nguyen, C., Corbett, J. G., ...
439 Kato, S. (2018, January). Clouds and the earth’s radiant energy system
440 (CERES) energy balanced and filled (EBAF) top-of-atmosphere (TOA)
441 edition-4.0 data product. *Journal of Climate*, 31(2), 895–918. Retrieved from

442 <https://doi.org/10.1175/jcli-d-17-0208.1> doi: 10.1175/jcli-d-17-0208.1
443 Marquardt, D. W. (1963, June). An algorithm for least-squares estimation of non-
444 linear parameters. *Journal of the Society for Industrial and Applied Mathemat-*
445 *ics*, 11(2), 431–441. Retrieved from <https://doi.org/10.1137/0111030> doi:
446 10.1137/0111030

447 Miller, R. L. (1997). Tropical thermostats and low cloud cover. *Journal of Climate*,
448 10(3), 409–440. doi: 10.1175/1520-0442(1997)010<0409:TTALCC>2.0.CO;2

449 Myers, T. A., Scott, R. C., Zelinka, M. D., Klein, S. A., Norris, J. R., & Caldwell,
450 P. M. (2021). Observational constraints on low cloud feedback reduce un-
451 certainty of climate sensitivity. *Nature Climate Change*, 11(6), 501–507.
452 Retrieved from <http://dx.doi.org/10.1038/s41558-021-01039-0> doi:
453 10.1038/s41558-021-01039-0

454 Norris, J. R., & Iacobellis, S. F. (2005, November). North pacific cloud feedbacks in-
455 ferred from synoptic-scale dynamic and thermodynamic relationships. *Journal*
456 *of Climate*, 18(22), 4862–4878. Retrieved from [https://doi.org/10.1175/
457 jcli3558.1](https://doi.org/10.1175/jcli3558.1) doi: 10.1175/jcli3558.1

458 Norris, J. R., & Weaver, C. P. (2001). Improved techniques for evaluating GCM
459 cloudiness applied to the NCAR CCM3. *Journal of Climate*, 14(12), 2540–
460 2550. doi: 10.1175/1520-0442(2001)014<2540:ITFEGC>2.0.CO;2

461 North, G., & Kim, K.-Y. (2017). *Energy balance climate models*. Weinheim, Ger-
462 many: Wiley-VCH.

463 Peters, M. E., & Bretherton, C. S. (2005). A simplified model of the Walker circula-
464 tion with an interactive ocean mixed layer and cloud-radiative feedbacks. *Jour-*
465 *nal of Climate*, 18(20), 4216–4234. doi: 10.1175/JCLI3534.1

466 Pierrehumbert. (1995, may). Thermostats, Radiator Fins, and the Local Runaway
467 Greenhouse. *Journal of the Atmospheric Sciences*, 52(10), 1784–1806. Re-
468 trieved from [http://journals.ametsoc.org/doi/10.1175/1520-0469\(1995\)
469 052%3C1784:TRFATL%3E2.0.CO;2](http://journals.ametsoc.org/doi/10.1175/1520-0469(1995)052%3C1784:TRFATL%3E2.0.CO;2) doi: 10.1175/1520-0469(1995)052<1784:
470 TRFATL>2.0.CO;2

471 Pierrehumbert, & Swanson. (1995, jan). Baroclinic Instability. *Annual*
472 *Review of Fluid Mechanics*, 27(1), 419–467. Retrieved from [http://
473 fluid.annualreviews.org/cgi/doi/10.1146/annurev.fluid.27.1.419](http://fluid.annualreviews.org/cgi/doi/10.1146/annurev.fluid.27.1.419)
474 doi: 10.1146/annurev.fluid.27.1.419

475 Rutan, D. A., Kato, S., Doelling, D. R., Rose, F. G., Nguyen, L. T., Caldwell,
476 T. E., & Loeb, N. G. (2015, June). CERES synoptic product: Methodol-
477 ogy and validation of surface radiant flux. *Journal of Atmospheric and Oceanic*
478 *Technology*, 32(6), 1121–1143. Retrieved from [https://doi.org/10.1175/
479 jtech-d-14-00165.1](https://doi.org/10.1175/jtech-d-14-00165.1) doi: 10.1175/jtech-d-14-00165.1

480 Sellers, W. D. (1969, jun). A Global Climatic Model Based on the Energy
481 Balance of the Earth-Atmosphere System. *Journal of Applied Meteorol-*
482 *ogy*, 8(3), 392–400. Retrieved from [http://journals.ametsoc.org/
483 doi/abs/10.1175/1520-0450\(1969\)008\(0392:AGCMBO\)2.0.CO;2](http://journals.ametsoc.org/doi/abs/10.1175/1520-0450(1969)008(0392:AGCMBO)2.0.CO;2)
484 [http://journals.ametsoc.org/doi/
485 10.1175/1520-0450\(1969\)008\(0392:AGCMBO\)2.0.CO;2](http://journals.ametsoc.org/doi/10.1175/1520-0450(1969)008(0392:AGCMBO)2.0.CO;2) doi:
486 10.1175/1520-0450(1969)008<0392:AGCMBO>2.0.CO;2

487 Sherwood, S. C., Webb, M. J., Annan, J. D., Armour, K. C., Forster, P. M., Harg-
488 reaves, J. C., ... Zelinka, M. D. (2020, December). An assessment of earth’s
489 climate sensitivity using multiple lines of evidence. *Rev. Geophys.*, 58(4).

490 Siebesma, A. P., Bony, S., Jakob, C., & Stevens, B. (Eds.). (2020). *Clouds and*
491 *climate*. Cambridge University Press. Retrieved from [https://doi.org/10
492 .1017/9781107447738](https://doi.org/10.1017/9781107447738) doi: 10.1017/9781107447738

493 Stephens, G. L., O’Brien, D., Webster, P. J., Pilewski, P., Kato, S., & Li, J.-I. (2015,
494 mar). The albedo of Earth. *Reviews of Geophysics*, 53(1), 141–163. Re-
495 trieved from <http://doi.wiley.com/10.1002/2014RG000449> doi: 10.1002/
496 2014RG000449

- 497 Stevens, B., & Brenguier, J.-L. (2009). Cloud-controlling factors: low clouds.
498 In J. Heintzenberg & R. J. Charlson (Eds.), *Clouds in the perturbed climate*
499 *system* (chap. 8). The MIT Press. Retrieved from [https://doi.org/](https://doi.org/10.7551/mitpress/9780262012874.001.0001)
500 [10.7551/mitpress/9780262012874.001.0001](https://doi.org/10.7551/mitpress/9780262012874.001.0001) doi: 10.7551/mitpress/
501 [9780262012874.001.0001](https://doi.org/10.7551/mitpress/9780262012874.001.0001)
- 502 Stevens, B., & Schwartz, S. E. (2012, May). Observing and modeling earth's energy
503 flows. *Surveys in Geophysics*, *33*(3-4), 779–816. Retrieved from [https://doi](https://doi.org/10.1007/s10712-012-9184-0)
504 [.org/10.1007/s10712-012-9184-0](https://doi.org/10.1007/s10712-012-9184-0) doi: 10.1007/s10712-012-9184-0
- 505 Zelinka, M. D., Myers, T. A., McCoy, D. T., Po-Chedley, S., Caldwell, P. M., Ceppi,
506 P., ... Taylor, K. E. (2020, January). Causes of higher climate sensitivity in
507 CMIP6 models. *Geophys. Res. Lett.*, *47*(1).